Research Journal of Applied Sciences, Engineering and Technology 12(11): 1112-1122, 2016
DOI:10.19026/rjaset.12.2852
ISSN: 2040-7459; e-ISSN: 2040-7467

Submitted: October 22, 2015 Accepted: January 5, 2016 Published: June 05, 2016

Research Article

Automated Demodulation of Amplitude Modulated Multichannel Signals with Unknown Parameters Using 3D Spectrum Representation

[1]Dmitriy Skopin and [2]Jamil Al-Azzeh
[1]Department of Biomedical Engineering, Southwest State University, Kursk, 305040, Russia
[2]Department of Computer Engineering, Al Balqa Applied University, Amman, 11134, Jordan

Abstract: In current research, new method of automated demodulation of amplitude modulated multichannel signals transmitted with unknown parameters has been proposed and tested. The method is perspective and actual because demodulation is an ill-posed problem when both the carrier and envelope signals are broadband and unknown. The innovative point of this study is the elaboration of the method that enables the evaluation of unknown parameters of the AM signal. The method is based on a new approach called the 3D spectrum representation of AM signals, where the first dimension indicates the allocation of carrier frequencies, the second indicates the band of message signal and the third is related to time. In this study, we report that the 3D representation enables to track unknown AM signal parameters, such as the carrier frequency, frequency of message signal and number of channels and apply demodulation techniques even for time-varying parameters of the signal. The results of the performed experiments indicate that the proposed method effectively performs the envelope detection and automated demodulation of multichannel AM signals.

Keywords: Amplitude modulation, carrier, demodulation, envelope, inference

INTRODUCTION

Amplitude Modulation (AM) is a method of transmitting signals, such as sound or digital information, in which the amplitude of the carrier wave is varied according to the message signal. AM is one of the simplest methods, in which a message signal can be modulated via a sinusoidal carrier wave, widely used in electronic communication and commercial radio broadcasting (Tokle *et al*., 2006). Moreover, there are two modulation schemes that can be used either with or without carrier suppression: double-sideband and Single-Sideband (SSB) (Billings, 2013). Currently, the AM multichannel signal is used in commercial radio broadcasts, where frequency ranges are allocated between radio stations. The band of the AM radio is known to be separated into three wave ranges: long range (153-279) kHz, medium (531-1,611) kHz with 9 kHz channel spacing for each range and short range (2.3-26.1) MHz; these ranges are divided into 14 broadcast bands (Forest *et al*., 2011).

Amplitude modulation and demodulation play an important role not only in communication technology but also in the speech recognition theory (Benzeghiba *et al*., 2007), electric motor faults diagnosis (Trajin *et al*., 2009), faults of wind turbine generators (Pons-Llinares *et al*., 2014) and three-phase machine fault detection (Kia *et al*., 2007). Thus, the development of methods for the automated detection, evaluation of unknown parameters and demodulation of AM signals is promising for further researches.

Currently, there are various approaches in demodulation techniques; coherent demodulation technique (Oppenheim and Schafer, 2009) is used in AM radio. On the other hand, an AM signal could be rectified without requiring a coherent demodulator when an envelope detector (a diode rectifier and a low-pass filter) is used. Another approach in demodulation techniques described in Benzeghiba *et al*. (2007), Oppenheim and Schafer (2009) is the product detector that multiplies the incoming signal by the signal of a local oscillator with the same frequency and phase as the carrier of the incoming signal. This technique will retrieve the original audio signal after filtering; moreover, it can decode both AM and SSB. If the phase could not be determined using this technique, a more complex setup would be required.

Some popular amplitude demodulation techniques include Hilbert transform (Potamianos *et al*., 1994) and Teager energy operator (Maragos *et al*., 1992;

Corresponding Author: Dmitriy Skopin, Department of Biomedical Engineering, Southwest State University, Kursk, 305040, Russia

Salzenstein and Boudraa, 2009; Diop *et al*., 2011; Alam *et al*., 2013; Zeng *et al*., 2014). Furthermore, for the three-phase system, the Concordia transform can be employed to perform demodulation (Potamianos *et al*., 1994). Several demodulation techniques, such as the diode detector or product demodulator, can be used to demodulate the AM multichannel signal, but, prior to demodulation, the desired carrier frequency needs to be separated from the spectrum. A simple method to do this would be to construct a set of band-pass filters. However, constructing filters require "a priori" parameters of the AM multichannel signal, such as the number of channels, frequencies of carriers and message signal bandwidth for each channel. For unknown or time-varying parameters, constructing such filters becomes an ill-posed problem.

This study proposes an innovative technique for the measurement of unknown parameters of multichannel AM signals in real time mode using a novel transform called the 3D spectrum representation. The first dimension of this transform indicates the frequencies of carriers for all channels of the original multichannel AM signal. The second dimension carries out information about the frequencies of the message signals, whereas the third one is related to time. Thus, the proposed method enables the real-time detection and tracking of parameters of the multichannel AM signal that allows the use of traditional methods of demodulation. Note that the tracking of the carrier frequency enables the construction of the Band-pass filter and the separation of different channels of the AM signal, evaluation of the message signal bandwidth and envelope detection using the traditional diode rectification and a low-pass filter. The approached technique is noise robust because the energy of the no modulated noise has no representation in the 3D spectrum surface and is ignored during demodulation. The method is independent to the physical transmission media and can be used for both the wireless and wire communications.

MATERIALS AND METHODS

This joint research was conducted in Southwest State University that located in Kursk, Russia and in Balqa Applied University, Amman, Jordan from 12 September of 2013 until 16 March of 2015. In this study, the original continuous time amplitude modulated multichannel signal is denoted as $x(t)$. During the sampling process, the original signal with a sample rate F_s during t_s seconds is transformed into discrete time signal $x[n]$. that contains N_s samples, which is given as follows:

$$N_s = F_s \cdot t_s \tag{1}$$

By dividing the signal $x[n]$. into a set of no overlapped windows of size N_{step} samples, the total number of windows N_w is defined according to Eq. (2) as follows:

$$N_w = \frac{N_s}{N_{step}} \tag{2}$$

Equation (3) illustrates the segmentation process of the signal X[n] into the set of N_w windows as follows:

$$\begin{aligned} x_d^w[n] &= x_d^w[0 : N_{step} - 1] \\ &= x[d \cdot N_{step} : (d+1) \cdot N_{step} - 1] \end{aligned} \tag{3}$$

where, ":" denotes the range of indices "from: to," "d" is the index of the window, d = 0: N_w.

According to Equation 4, the index d of each window is related to the current time t_{cur} of the original signal $x(t)$. as follows:

$$t_{cur} = d \cdot \frac{t_s}{N_w} \tag{4}$$

The short-time Fourier Transform (STFT) (Paliwal and Alsteris, 2005; Al-Azzeh *et al*., 2015) of the signal $x_d^w[n]$ is defined according to the formula 5 as follows:

$$\dot{X}(\tau, \omega) = \sum_{n=0}^{N_{step}} x_d^w \cdot W[n - N_{segm}] \cdot e^{-j\omega n} \tag{5}$$

where, W is the windowing function of length N_{segm} samples.

On a physical level, $\dot{X}(\tau, \omega)$ is an image limited by size $\tau_{\max} = \frac{N_{step}}{Fs}$ $\omega_{\max} = \frac{Fs}{2}$.

The $X(\tau, \omega)$ image contains information about harmonics allocation of the signal $x_d^w[n]$ at a certain time moment τ and each row of this image indicates the evolution of harmonic ω during that time.

The 2D spectrum representation $\ddot{X}(\omega_r, \omega)$ of the signal x_d^w[n] is defined in the current work as the Discrete Fourier Transform (DFT) of $\dot{X}$ (τ,:), as illustrated in Eq. (6):

$$\ddot{X}(\omega_r, \omega) = \sum_{n=0}^{\tau_{\max}} \dot{X}(n, \omega) \cdot e^{-\frac{j2\pi\omega_r n}{\tau_{\max}}} \tag{6}$$

The $\ddot{X}(\omega_r, \omega)$ is a 2D image in which each pixel is characterized by two dimensions: ω_r is the frequency of the message signal and ω is the frequency of the carrier.

Considering the fact that $\dot{X}(n, \omega)$ is the STFT of the signal $X_d^w[n]$, signal $X_d^w[n]$, is a window with the number "d" of the original signal $X[n]$ and the index d is related to time according to Eq. (4), using all the ranges of d from zero to N_w-1, the 2D transformation (6) can be represented as a 3D transformation (7):

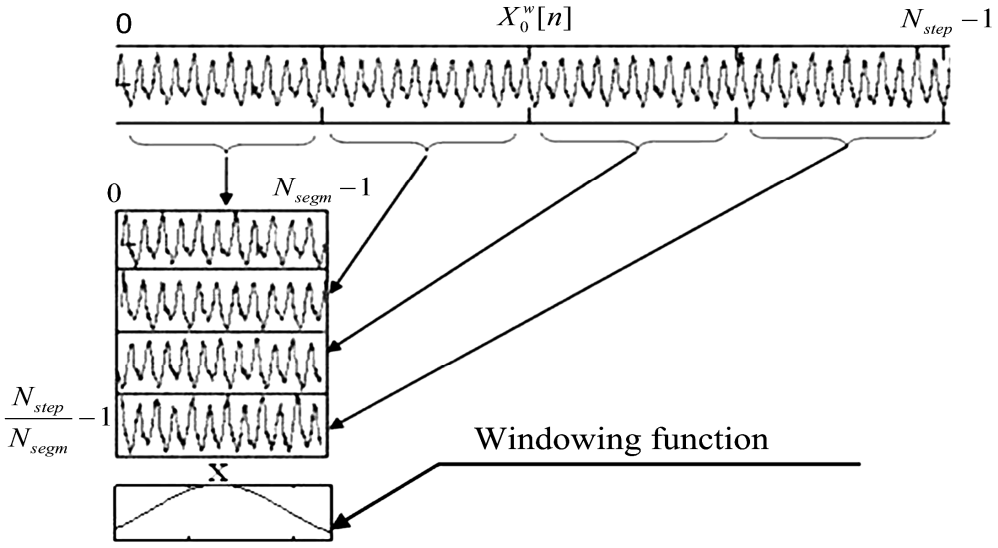

Fig. 1: Segmentation of x_0^w [n] signal into the set of rows

$$\ddot{X}(\omega_r,\omega,d)=\sum_{n=0}^{\tau_{\max}}\dot{X}(n,\omega,d)\cdot e^{-\frac{j2\pi\omega_r n}{\tau_{\max}}} \quad (7)$$

On a physical level, $\ddot{X}(\omega_r,\omega,d)$ describes the 3D space where the position of each point of the space is related to the frequency of the message signal, frequency of the carrier and time variable. The algorithm that implements transformation 7 is as follows:

Step 1: Let $x(t)$ be the original monochromatic AM signal in which the harmonic with the frequency ω_m is modulated using the carrier with the frequency ω_c. After sampling the $x(t)$ with a sampling rate Fs, the signal was converted into a discrete form $x(t)$. Using Eq. (3), first, the signal $x(t)$ is divided into a set of windows $x_d^w[n]$. Second, assume that the current value of d is zero. Thus, the current window is $x_0^w[n]$.

Step 2: x_0^w[n] is divided into a set of segments of length N_{segm} samples; then, each segment is multiplied by a windowing function W (Fig. 1).

Each row of the image shown in Fig. 1 consists of N_{segm} samples of the signal $x_0^w[n]$ totally formed $\frac{N_{step}}{N_{segm}}$ rows. The DFT in rows provided according to Equation 5 transforms the original image into the STFT.

Assume that the original continuous time AM signal is defined as follows:

$$x(t)=x_m(t)\cdot\cos(2\pi f_c t), \quad (8)$$

where, $x_m(t)$ is the message signal, f_c is the frequency of the carrier.

The STFT can be expressed as the set of Fourier transforms of $x_i(t)$ signal defined as the product of $x(t)$ and windowing functions W_i as follows:

$$x_i(t)=x(t)\cdot W_i \quad (9)$$

The Fourier transform $X_i(f)$ for each window W_i is related to the Fourier transform $X_m(f)$ of the message signal as follows:

$$X_i(f)=\frac{1}{2}X_m(f-f_c)+\frac{1}{2}X_m(f+f_c) \quad (10)$$

Now, consider only the positive part of $X_i(f)$ spectrum. Suppose that the message signal is represented by a single harmonic with the frequency f_m, the Equation obtained is as follows:

$$x_m(t)=\cos(2\pi f_m t) \quad (11)$$

In this case, the Fourier transform of $X_i(f)$ consists of two harmonics with frequencies f_c-f_m (lower sideband) and f_c+f_m (upper sideband). Since the amplitude of the message signal varied according to Eq. (11), the amplitudes of the upper and lower sidebands also vary according to the same law and the STFT of $x(t)$ signal is represented as two sinusoids. Assume that $f_c>>f_m$ or the value of f_m is less than the frequency resolution of the Fourier Transform. In this case, the resulting spectrogram will be represented as a single sinusoid with the frequency f_m located in the position f_c (Fig. 2).

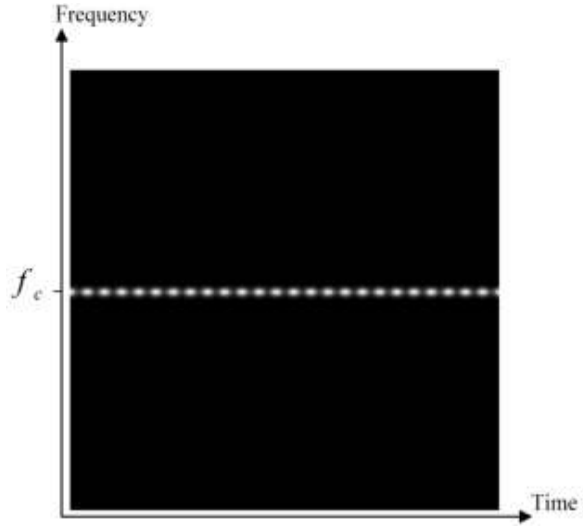

Fig. 2: The spectrogram of the signal $x(t)$

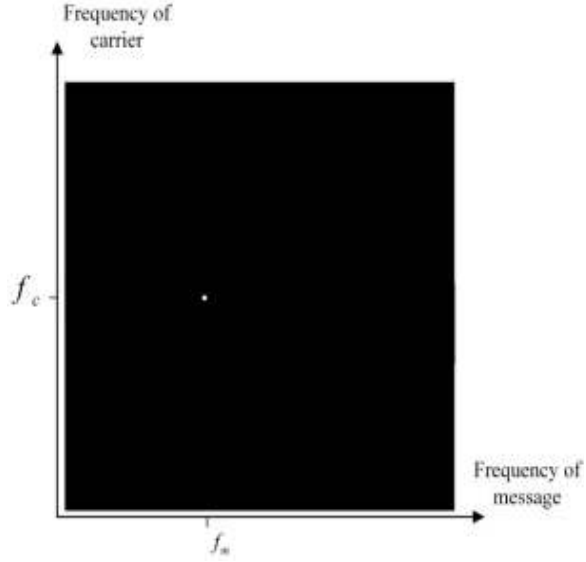

Fig. 3: Particular case of 3D transform for d = 0 of the signal $x_0^w[n]$

Step 3: Using transformation 7, the signal $X_0^w[n]$ transformed into a 3D representation $\ddot{X}(\omega_r, \omega, 0)$, where ω_r is the frequency of the modulating signal, ω is the frequency of the carrier and index 0 indicates the time. As shown above, the spectrogram of $x(t)$ model contains a single harmonic with the frequency f_m. Note that the result of transformation 7 for $x(t)$ signal is represented as a single point since the energy of the signal in the position of f_c is concentrated in the position f_m of $\ddot{X}(\omega_r, \omega, 0)$ space (Fig. 3).

For convenience, we have rearranged the location of the coordinate axes in the following sections of the paper according to the coordinate system of the computer images, where the vertical axis is directed from the top to bottom.

Since the parameters of the monochromatic signal $x(t)$ are time-invariant, the position of the point is also time invariant. For the time-varying parameters $x(t)$, the proposed 3D spectrum $\ddot{X}(\omega_r, \omega, d)$, representation tracks the parameters of the modulating signal and carrier for each time value "d."

The maximum frequencies of the carrier and message signals that can be detected by the proposed method are limited by the values $f_{carrier}^{max}$ and $f_{message}^{max}$. These parameters can be evaluated using Eq. (12) and (13):

$$f_{carrier}^{\max} = \frac{F_s}{2} \tag{12}$$

$$f_{message}^{\max} = \frac{F_s}{2 \cdot N_{segm}} \tag{13}$$

The frequency resolution of the method can be expressed with reference to the properties of the DFT, where the first harmonic frequency of a signal related to its duration. The frequency resolution of the carrier is denoted as R_c (Hz) and numerically described by Eq. (14) as follows:

$$R_c = \frac{F_s}{N_{segm}} \tag{14}$$

The frequency resolution R_m (Hz) of the message signal is expressed by Eq. (15) as follows:

$$R_m = \frac{F_s}{N_{step}} \tag{15}$$

When the time resolution R_t (seconds) is given by 16, which is as follows:

$$R_t = \frac{t_s}{N_{segm}} \tag{16}$$

The demodulation of the signal can be performed using well-known methods of signal processing. In the current work, a model of an envelope detector is used, which is represented by a rectifier, digital Infinite Impulse Response (IIR) passband and low-pass filters that are connected according to Eq. (17):

$$x_d[n] = H_d^{lp} * \left| H_d^{bp} * x_d^w[n] \right| \tag{17}$$

where, | | denotes modulus operator to perform full wave rectification, $x_d^w[n]$ is the segment of the original multichannel AM signal, * is the operator of convolution and H_d^{lp} and H_d^{bp} are the impulse responses of the digital low-pass and band-pass filters, respectively.

The impulse responses H_d^{bp} and H_d^{lp} can be computed using any standard procedure of the digital filter design (Libbey, 1994; Oppenheim and Schafer, 2009).

Note that signal processing according to Eq. (17) related to the time domain when the evaluation of AM signal parameters using the 3D spectrum representation related to the frequency domain.

The parameter of the filter design algorithm for the low-pass filter: the cutoff frequency of the low-pass filter ω_x^{lp} defined according to the maximum value of the vertical position of the signal on the 3D space; for band-pass filter the cutoff frequencies can be evaluated according to Eq. (18):

$$\omega_c^{bp} = x \pm \omega_c^{lp} \tag{18}$$

where, x is the frequency of the carrier related to the horizontal position of a point on the 3D spectral surface.

The following algorithm of the features extraction of AM multichannel signal parameters has been used in the current project:

- For each window d of signal $X[n]$, the threshold parameter tr_d is defined as follows:

$$tr_d = 0.08 \cdot \max\left\{\ddot{X}(\omega_r, \omega, d)\right\} \tag{19}$$

- For each window d, define the number of channels ch_{max} as the number of columns of the $\ddot{X}(\omega_r, \omega, d)$ image with the brightness of pixels above tr_d level.
- For each channel i, i = 1: ch_{max}, evaluate the following features of the signal using the threshold value tr_d: for the message signal parameter $\omega_{r,max,i}^d$- the maximum frequency of the message signal; for the carrier: the minimum and maximum frequencies $\omega_{min,i}^d$ and $\omega_{max,i}^d$.
- For each channel i, i = 1 : ch_{max} i of the window d, provide demodulation according to Equation 17 using the following parameters of the filters: for H_d^{lp} filter-cutoff frequencies at $\omega_{min,i}^d$ and $\omega_{max,i}^d$; for H_d^{lp} filter: - cutoff frequency $\omega_{r,max,i}^d$.

RESULTS AND DISCUSSION

The ability of the suggested approach to evaluate unknown parameters of the multichannel amplitude modulated signal has been tested using the synthetic signal V(t). The signal is represented as the sum of the three components (channels) that are particularly cross linked in time:

$$V(t) = x_1(t) + x_2(t) + x_3(t) \tag{20}$$

where,

$$x_1(t) = (1 + 0.5\sin(2\pi 3000t) \times \cos(2\pi(400000 - 37500t)t),$$
$$x_2(t) = (1 + 0.9\sin(2\pi 1200t^2) \times \cos(2\pi(200000 + 42500t)t),$$
$$x_3(t) = \cos(2\pi 220000t).$$

The first component $x_1(t)$ is the modulated signal with the time-varying frequency of the carrier with the following parameters: the initial carrier frequency 400 KHz, frequency of message signal 3 KHz. The second component $x_2(t)$ is the modulated signal with the time-varying frequencies of the carrier and message signals: the initial frequency of the message signal 1200 Hz, initial frequency of the carrier 200 KHz. Third component $x_3(t)$ is the no modulated signal with the time-invariant frequency 220 KHz. During experiments, the following parameters of the demodulation algorithm have been selected: a sample rate F_s = 1 MHz, the duration of signal sampling t_s-4 seconds; the size N_{step} of the window-40000 samples and the size of the windowing function N_{segm}-100 samples. According to Eq. (2), the total number of windows N_w is defined as 100, the duration of the signal in each window becomes equal to 0.04 seconds, as shown in Equation 4. The selected parameters of the synthetic signal will theoretically give 10 KHz of the spectral resolution of the carrier with a percentage error of 2%, 25Hz of the message signal resolution with a percentage error of 0.5% and 0.04 seconds of the time resolution with a percentage error 0.8%.

To obtain the parameters of the multichannel AM signal, we have applied transformation 7 for various values of d from 0 to 99. For each value of d, transformation 7 returns the image with the parameters of the modulated signal. Figure 4 indicates the spectrogram of the signal 20 and the projection of the 3D spectrum into the 2D space for the values of d = 40 that related to the time moment equal to 1.6 seconds. The original size of the image shown in Fig. 4b for the selected parameters of the signal processing algorithm is defined according to the Fourier transform properties as 200×50 pixels. To display the image with a resolution of 500×500 pixels, the bilinear image scaling algorithm (Gonzales and Woods, 2008) has been applied.

According to Equation 20, the parameters of the AM signal for the mentioned time moment are as follows: the carrier frequency of the first channel $x_1(t)$ 340 KHz, message frequency 3KHz; carrier frequency of the second signal $x_2(t)$ 268 KHz, message frequency 1.92 KHz. The time–frequency domain of the signal $V(t)$ is shown in Fig. 4a. This Figure demonstrates three components of the signal: $x_1(t)$ with a falling frequency, $x_2(t)$ with an increasing frequency and time-invariant frequency of $x_3(t)$ component. However, the spectrogram has no representation of the modulating

frequency and visually, all three components are observed not to be modulated. Figure 4b shows the $\ddot{X}(\omega_r, \omega, 40)$ image in which the modulated components of the signal $V(t)$ are represented as white spots. Note that the estimated parameters of $x_1(t)$ and $x_2(t)$ components are near to the theoretical parameters. Moreover, the last unmodulated component $x_3(t)$ has not been presented in the image since the frequency of the message signal of this component is zero.

To study the evolution of signal parameters during time, we have applied the algorithm of the AM signal feature extraction described in the section 2. For the selected parameter d = 40, the algorithm returned the following signal parameters: the number of channels 2, parameters of the first channel: $\omega_{min,1}^{40}$= 340 KHz, $\omega_{max,1}^{40}$ = 370 KHz, $\omega_{r,max,1}^{40}$ = 3025Hz; parameters of the second channel: $\omega_{min,2}^{40}$ = 260 KHz, $\omega_{max,2}^{40}$ = 290 KHz, $\omega_{r,max,2}^{40}$ = 1925Hz.

Parameters determined by the algorithm also demonstrate a valuable agreement with the theoretical values determined according to Equation 20. The application of the algorithm for all values of d from 0 to 99 enables to illustrate the evolution of $\ddot{X}(\omega_r, \omega, 0{:}\ 99)$ parameters in the 3D space (Fig. 5c). Furthermore, the proposed method enables analyzing the parameters

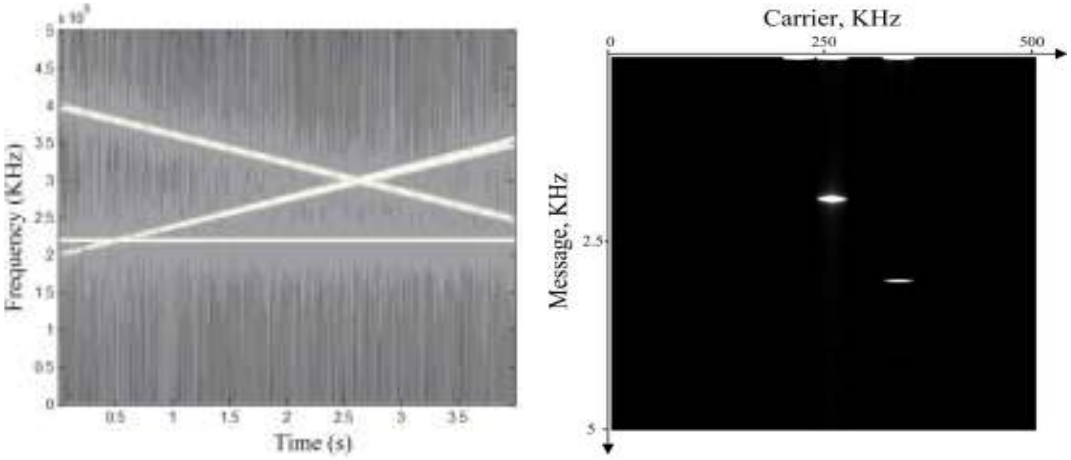

(a) (b)

Fig. 4: The spectrogram (a) of original signal $V(t)$ and (b) $\ddot{X}(\omega_r, \omega, 40)$ image

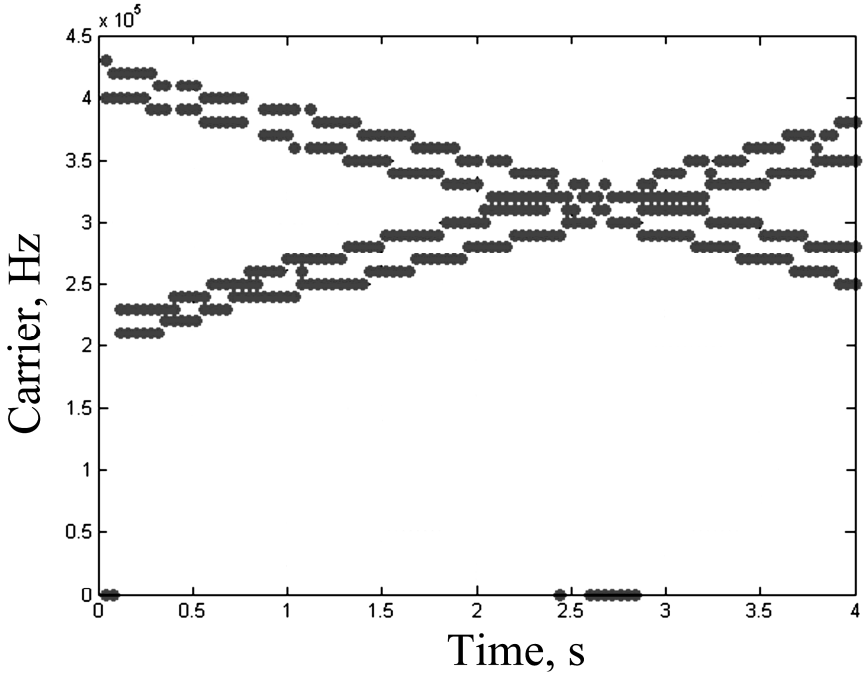

(a)

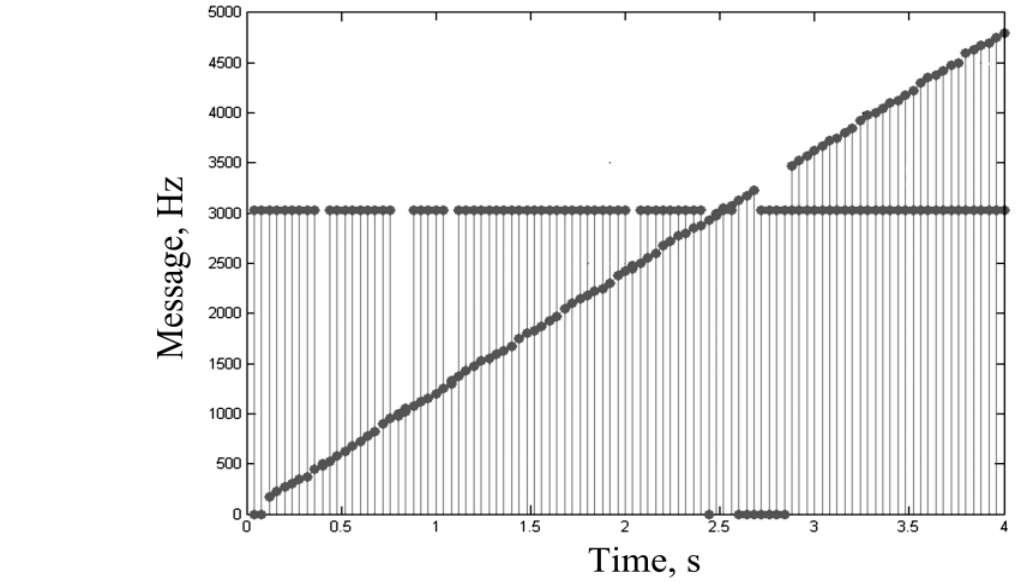

(b)

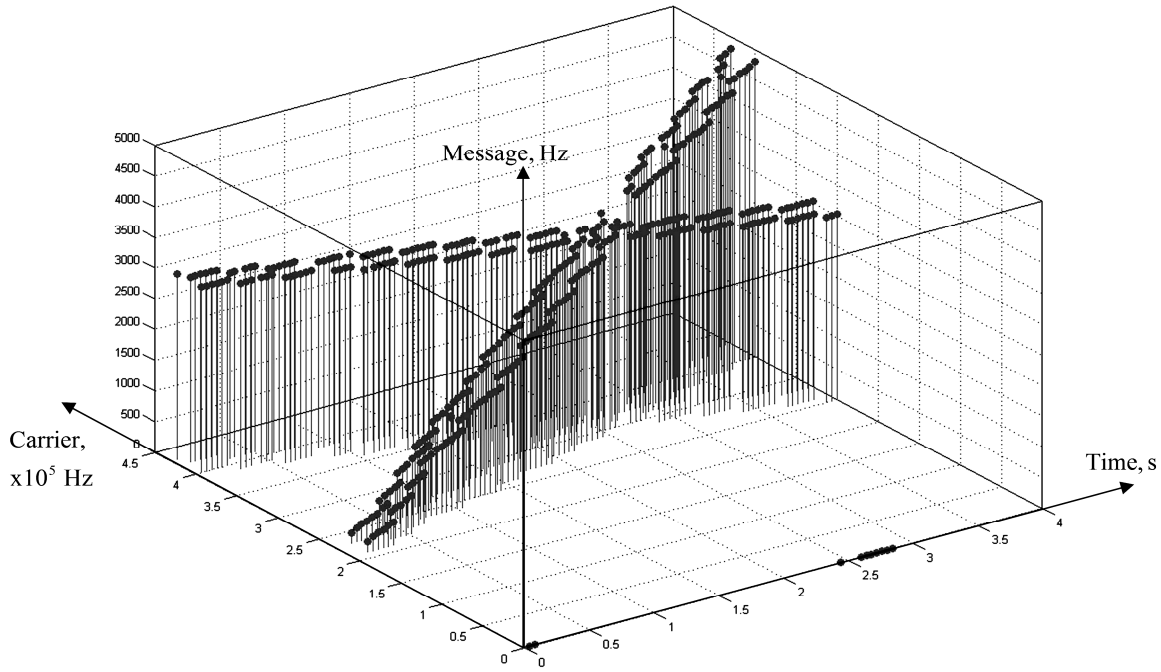

(c)

Fig. 5: Representation of synthetic signal using 3D spectrum representation; (a): Projection of $\ddot{X}(\omega_r, \omega, d)$ into time frequency domain of carriers; (b): Projection into time-frequency domain of message signal; (c): 3D representation of $\ddot{X}(\omega_r, \omega, d)$

of the carriers separately from the parameters of the message signals.

In addition, note that the parameters of the carriers and message signals coincide with the parameters of the synthetic signal.

To address the accuracy of the method, the pilot study was performed to evaluate the percentage error in measuring the message frequency. During the study, the frequencies of the modulating signals were evaluated using the proposed algorithm and then compared with the true values computed using the model of the signal described by Eq. (20). Experimentally, the error does not exceed 5% theoretical value (Table 1).

In addition, we have applied the proposed method of the 3D spectrum representation to a multichannel amplitude modulated speech sound. There is an important difference between the synthetic signal created according to Equation 20 and the real sounds,

Table 1: Accuracy of proposed method

Test number	Evaluated value, Hz	True value, Hz	Percentage error, %
1.	1200	1200	0.00
2.	1925	1920	0.26
3.	2270	2280	0.43
4.	2520	2520	0.00
5.	3125	3120	0.17
6.	3850	3840	0.26
7.	4195	4200	0.12
8.	4450	4440	0.12
9.	4600	4580	0.24
10	4690	4680	0.21

Average percentage error 0.18%, Average accuracy 99.82%

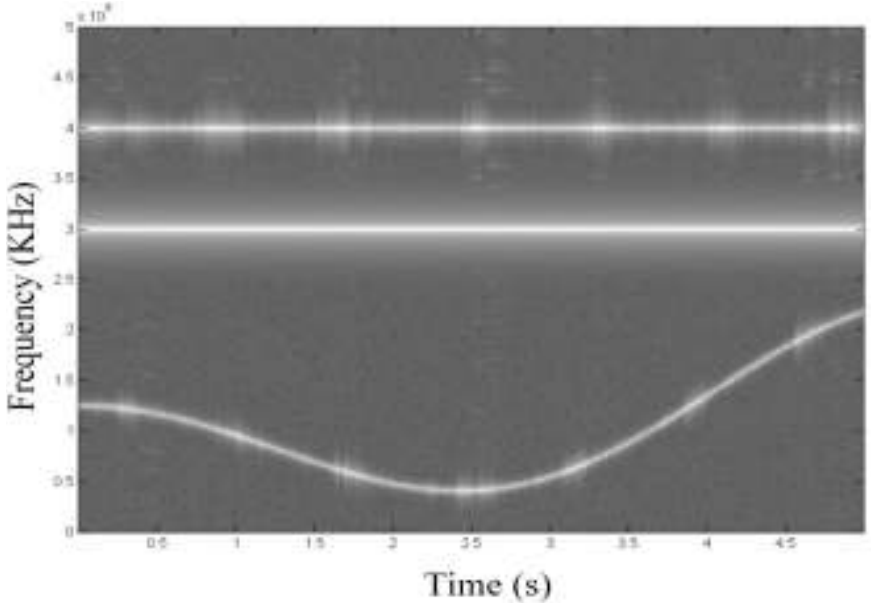

Fig. 6: The spectrogram of the $x(t)$ signal

such as speech, treated here. The synthetic sound contains a single time-scale of modulation, whereas the real sound naturally contains modulation at multiple time-scales (Turner and Sahani, 2011).

This section applies the 3D spectrum representation to the amplitude modulated signal $x(t)$ that includes three channels $x_1(t)$, $x_2(t)$ and $\varepsilon(t)$. The message signal $x_1(t)$ is a speech signal limited by a bandwidth of 5KHz that is modulated with a carrier of 400 Hz, whereas the message signal $x_2(t)$ is a speech signal limited by a bandwidth 3.5 KHz modulated with a time-varying carrier of $x_c(t)$ with an unknown frequency. The third channel $\varepsilon(t)$ is a high amplitude nonmodulated noise located in the band from 290 KHz to 310 KHz. The model of the audio signal is shown as follows:

$$x(t) = x_1(t) \cdot \cos(2 \cdot \pi \cdot 400000t) + x_2(t) \cdot x_c(t) + \varepsilon(t) \quad (21)$$

Figure 6 illustrates the spectrogram of the signal $x(t)$.

Signals $x_1(t)$ and $x_2(t)$ are English speech sounds of counting from one to ten of two different people. We have applied the following parameters of the 3D spectrum estimation: a sample rate F_s = 1 MHz, duration of signal sampling t_s-4 seconds; the size N_{step} of the window: 40000 samples, size of the windowing function: N_{segm} 100 samples. During experiments, the original message signals $x_1(t)$ and $x_2(t)$ were saved in different wave files to use it as a referenced data during the testing of the proposed method. Figure 7a shows the results of transformation 7 and the feature extraction algorithm as the $\ddot{X}(\omega_r, \omega, d)$ image. The figure illustrates a good agreement between the measurement of the carrier frequencies using the suggested method and spectrogram 6. Furthermore, since the noise component $\varepsilon(t)$ is unmodulated, its energy is absent in the 3D spectrum representation (Fig. 7a). To show the identity of estimating the frequency of the information signal using the proposed algorithm, we have used the spectrogram of the $x_2(t)$ (Fig. 7b) and projection of the $\ddot{X}(\omega_r, \omega, d)$ image into the time–frequency domain (Fig. 7c). The analysis of Fig. 7b and 7c enables us to conclude that the measurement of the carrier frequency using the proposed method shows good agreement with the standard measurement by spectrogram.

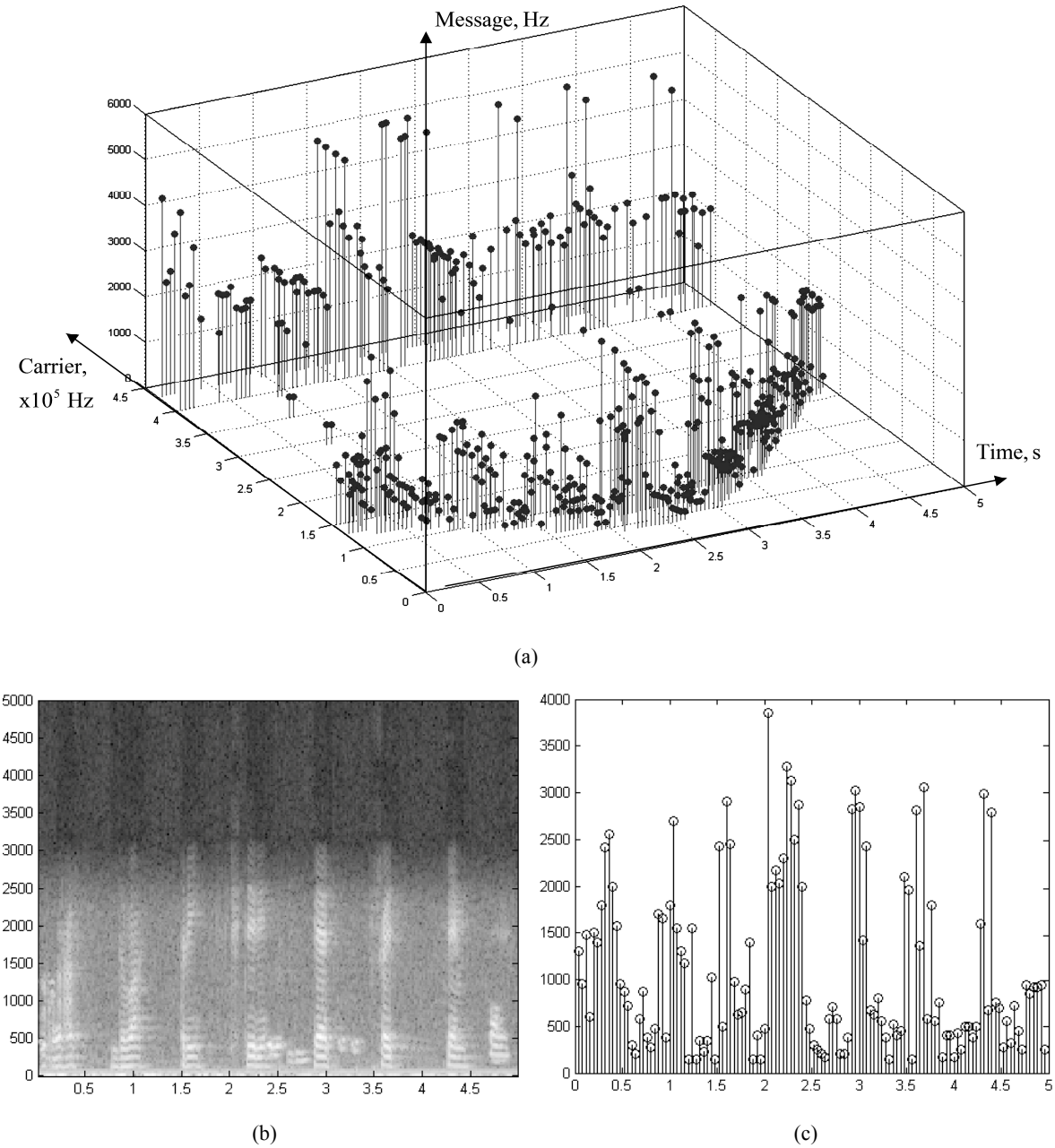

Fig. 7: The 3D spectrum representation; (a): $x(t)$ signal; (b): spectrogram of original $x_2(t)$ signal; (c): Tracking the $x_2(t)$ signal frequency extracted by proposed algorithm

The demodulation technique was applied according to Eq. (17). To address the overall performance of the proposed method of the demodulation of the AM multichannel signal with unknown parameters, the Perceptual Evaluation of Audio Quality (PEAQ) algorithm (Spanias *et al*., 2007) has been used in the current work. The PEAQ is a standardized algorithm for objectively measuring the perceived audio quality. It was originally released as International Telecommunication Union (ITU) recommendation in 1998 and last updated in 2001. Using a method of the PEAQ, we have tested a degradation of audio quality using proposed method of demodulation. The source wave files with signals $x_1(t)$ and $x_2(t)$ has been used as a referenced file for the PEAQ model. The demodulated signals x_1^d(t) and x_2^d(t) are used as the testing files. The Objective Difference Grade (ODG) is calculated by the perceptual evaluation of the audio quality algorithm. It corresponds to the subjective difference grade used in human-based audio tests. The voices of 21 volunteers (from 18 to 21 years old) are used for PEAQ evaluation. The results returned by the ODG grade show numerical values of -1.28 (standard deviation 0.048) for x_1^d(t) and -1.59 (standard deviation 0.069)

for $x_1^d(t)$ signals. Both numerical values refer to the impairment description "Perceptible, but not annoying." Thus, the proposed method of AM signal measurements and the demodulation is an innovative approach that can be recommended in the implementation of various signal analysis algorithms and digital communication systems.

CONCLUSION

The demodulation of multichannel AM signals is a well-known problem that can be solved using numerous methods. However, the application of demodulation techniques requires the parameters such as the number of channels, frequencies of carriers and message signals for each channel of the signal. Demodulation is an ill-posed problem when both the carrier and envelope signals are broadband, unknown, or in the case of time-varying parameters of the signal.

This study has introduced a new perspective on demodulation, using the 3D spectrum representation approach. This perspective directly led to the development of an algorithm called the AM signal feature extraction, which enables the detection of all the required parameters of the AM signal, such as the number of channels, instantaneous frequencies of carriers and message signal and the tracking of parameters during that time. The algorithm enables real-time demodulation of all channels even for the time-varying frequency of the carrier and message signal. This plays an important role in coupled researches related to the demodulation of AM signals in the fields of data transmission, speech recognition and acoustic diagnostics of mechanism faults. Using the synthetic signal, we demonstrated that the method was robust to detect the parameters of different signals that are particularly cross linked during time. The proposed 3D spectrum representation ignores the nonmodulated components of the multichannel signal and in the case of "meeting" the frequencies of different carriers, the algorithm fails to evaluate the signal parameters only during the time when the two different channels are transmitting using equivalent carrier frequencies (Fig. 5b). In the application of the natural sounds demodulation, the method illustrates an acceptable quality of results according to the PEAQ. However, the feature extraction algorithm indicates about 5% of errors during the tracking of signal parameters, which can be explained by the fact that during pronunciation, a human speech contains pauses, which lead to the appearance of nonmodulated signal components that are ignored by the 3D spectrum approach.

The 3D spectrum representation and features extraction algorithm also lends itself naturally to changes in the assumptions about the carrier and modulation content and thus the current algorithm may form the basis of useful extensions.

REFERENCES

Alam, M.J., P. Kenny and D. O'Shaughnessy, 2013. Smoothed nonlinear energy operator-based amplitude modulation features for robust speech recognition. Proceeding of the 6th International Conference on Non-Linear Speech Processing (NOLISP, 2013). Mons, Belgium, June 19-21, 7911: 168-175.

Al-Azzeh, J.S., M.E. Leonov, D.E. Skopin, E.A. Titenko and I.V. Zotov, 2015. The organization of built-in hardware-level mutual self-test in mesh-connected VLSI multiprocessors. Int. J. Inf. Tech., 3(2): 29-34.

Benzeghiba, M., R. De Mori, O. Deroo, S. Dupont, T. Erbes, D. Jouvet, L. Fissore, P. Laface, A. Mertins, C. Ris, R. Rose, V. Tyagi and C. Wellekens, 2007. Automatic speech recognition and speech variability: A review. Speech Commun., 49(10-11): 763-786.

Billings, S.A., 2013. Nonlinear System Identification: NARMAX Methods in the Time, Frequency, and Spatio-Temporal Domains. John Wiley and Sons Inc., Chichester, West Sussex, United Kingdom, pp: 320-322.

Diop, E.H.S., A.O. Boudraa and F. Salzenstein, 2011. A joint 2D AM-FM estimation based on higher order Teager-Kaiser energy operators. Signal Image Video Process., 5(1): 61-68.

Forest, D., L. Sterling, H. Christopher, C. O'Dell and M. Keith, 2011. The Biographical Encyclopedia of American Radio. Routledge, pp: 94-96, ISBN 0415995493.

Gonzales, R.C. and R.E. Woods, 2008. Digital Image Processing. 3rd Edn., Prentice Hall, Upper Saddle River, N.J., pp: 750-784.

Kia, S.H., H. Henao and G.A. Capolino, 2007. A high-resolution frequency estimation method for three-phase induction machine fault detection. IEEE T. Ind. Electron., 54(4): 2305-2314.

Libbey, R., 1994. Signal and Image Processing Sourcebook. Springer, US, pp: 450.

Maragos, P., J.F. Kaiser and T.F. Quatieri, 1992. On separating amplitude from frequency modulations using energy operators. Proceeding of the IEEE International Conference on Acoustics, Speech, and Signal Processing (ICASSP-92). San Francisco, CA, 2: 1-4.

Oppenheim, A.V. and R.W. Schafer, 2009. Discrete-Time Signal Processing. 3rd Edn., Prentice Hall Press, Upper Saddle River, NJ, USA, pp: 512-522.

Paliwal, K.K. and L.D. Alsteris, 2005. On the usefulness of STFT phase spectrum in human listening tests. Speech Commun., 45(2): 153-170.

Pons-Llinares, J., J. Antonino-Daviu, J. Roger-Folch, D. Moríñigo-Sotelo and O. Duque-Pérez, 2014. Mixed eccentricity diagnosis in inverter-fed induction motors via the adaptive slope transform of transient stator currents. Mech. Syst. Signal Pr., 48(1-2): 423-435.

Potamianos, A. and P. Maragos, 1994. A comparison of the energy operator and the Hilbert transform approach to signal and speech demodulation. Signal Process., 37(1): 95-120.

Salzenstein, F. and A.O. Boudraa, 2009. Multi-dimensional higher order differential operators derived from the Teager-Kaiser energy-tracking function. Signal Process., 89(4): 623-640.

Spanias, A., T. Painter and V. Atti, 2007. Quality Measures for Perceptual Audio Coding. In: Audio Signal Processing and Coding. Wiley-Interscience, pp: 401-407, ISBN 0471791474.

Tokle, T., M. Serbay, J.B. Jensen, Y. Geng, W. Rosenkranz and P. Jeppesen, 2006. Investigation of multilevel phase and amplitude modulation formats in combination with polarization multiplexing up to 240 Gb/s. IEEE Photonic. Tech. L., 18(20): 2090-2092.

Trajin, B., M. Chabert, J. Regnier and J. Faucher, 2009. Hilbert versus Concordia transform for three-phase machine stator current time-frequency monitoring. Mech. Syst. Signal Pr., 23(8): 423-2657.

Turner, R.E. and M. Sahani, 2011. Demodulation as probabilistic inference. IEEE T. Audio Speech, 19(8): 2398-2411.

Zeng, M., Y. Yang, J. Zheng and J. Cheng, 2004. Normalized complex Teager energy operator demodulation method and its application to fault diagnosis in a rubbing rotor system. Mech. Syst. Signal Pr., 50-51: 380-399.